SUPPLEMENTARY METHODS

Derivation of expression plasmids

pBT264 was a gift from Liqun Luo (Addgene plasmid #27438). [37] To generate pBT264-MBSacceptor, two 147 bp oligonucleotides (Supplementary Table 3) containing tough decoy (TuD) stem sequences and spacer fragments were annealed and ligated to pBT264 sequentially digested with BglII and MfeI. Two oligonucleotides containing SalI, ScaI, and NotI recognition sites, with or without a RNA polymerase III poly-T termination signal, were annealed and ligated to pKT2-Fah-U6-sgRNA-SBK [16] digested with SapI and EcoRI to generate pKT2-Fah-U6-TuDacceptor-pT and pKT2-Fah-U6-TuDacceptor-tail. To derive a TuD expression plasmid for *in vivo* TRAP-Seq, an NheI recognition sequence was added to the 5' end of the U6-TuDacceptor-pT sequence of pKT2-Fah-U6-TuDacceptor-pT by PCR. This amplicon was then inserted at the NheI site of pKT2-Fah-eGFP-L10a [2] to derive pKT2-Fah-eGFP-L10a-U6-TuDacceptor-pT.

pMiRCheck2 was a gift from Nicholas Hand. [38] MicroRNA sensor plasmids were derived by ligating annealed oligonucleotides containing tandem miRNA recognition sequences to pMiRCheck2 at the XhoI and NotI recognition sites located in the 3'UTR of the *Renilla* luciferase cDNA. Similarly, dual luciferase reporter plasmids for mouse 3'UTRs were generated by PCR-amplifying regions of interest and inserting amplicons into the XhoI/NotI cloning site of pMiRCheck2. Predicted miRNA binding sites within the inserted sequences were mutated via overlap PCR.

pGeneClip (Promega) shRNA expression plasmids were derived by ligating oligonucleotides encoding the mouse miR-374b hairpin or a negative control shRNA.

Cell growth assays

Hepa 1-6 mouse hepatoma cells were transfected with 1 μg of pGeneClip expression plasmids using Lipofectamine 3000, and were treated with 5 μg/mL puromycin for 7-10 days. After selection, equal numbers of cells were plated in 12-plates and cultured for one week. Cells were then fixed in paraformaldehyde and stained with 0.05% crystal violet.

For MEX3C inhibition experiments, Hepa 1-6 or Huh-7 cells were grown in 24-well plates and in the presence of triptolide (Sigma-Aldrich) for seven days. Cells were then fixed in paraformaldehyde and stained with 0.05% crystal violet.

High throughput DNA sequencing

Tough decoys in the TuDstd and TuDtail input libraries, and genomic DNA extracted from livers of *Fah*$^{-/-}$ mice, were amplified by two rounds of PCR to introduce Illumina capture and index sequences. Primer sequences are listed in Supplementary Table 3. In the first round of PCR, we performed four reactions using 200 ng of the plasmid library as template and eight separate reactions for each liver sample using 5 µg of genomic DNA as template. For each liver sample, the first round reaction products were pooled and 5 µL was used as template for the second PCR. Amplicons were gel purified, quantified using Agilent 2100 Bioanalyzer and Kapa SYBR Fast qPCR protocols, and sequenced using a 75-cycle Illumina NextSeq 500/550 High Output kit. The distance from the 5' end of the MBS1 sequence to the 3' end of the MBS2 sequence enabled quantification of TuDs by 84 sequencing cycles using a custom primer complementary to the 5' TuD stem sequence. The remaining 7 cycles were used for the sample index read.

For the TuD competition experiment, TuD sequencing libraries were generated from input pools and mouse liver gDNA as above. Libraries were paired-end sequenced using a 300-cycle MiSeq Nano Kit v2 with our custom 5' primer and a standard Illumina 3' primer. Forward and reverse reads were averaged for each TuD and animal.

Dataset integration

To combine results across experiments, we used raw sequencing counts and calculated TuD reads per million (rpm) for each sequencing replicate. Locally weighted regression scatterplot smoothing (LOWESS) was used to inform our selection of minimal read count thresholds for data to be included in downstream analyses. For each animal, smoothing was performed on the ratio of liver rpm to the mean plasmid rpm against the $\log_{10}$ of the total rpm using a bandwidth size of 1,500 TuDs. Minimum read count thresholds were selected at the lowest total rpm value corresponding to a

smoothed line slope of zero. TuD fold change values (liver/input plasmid library) were defined as the residuals from the smoothed line. Prior to dataset integration, TuD $\log_2$ fold change distributions of each liver sample were standardized by dividing each value by the sample standard deviation. Missing $\log_2$ fold change values across all livers were then imputed sequentially as follows until all missing values were substituted. For each TuD, AB, within each experiment:

If at least one value is present for AB, missing AB values are replaced by the AB mean.

If all AB values are missing, missing AB values are replaced by the mean BA value (i.e. its mirror).

If all values of AB and BA are missing, missing AB and BA values are replaced by sample medians.

The standardized and imputed TuD $\log_2$ fold change values were converted to the linear scale and distributions were then transformed using the RUV-4 method, [39] which leverages internal negative controls within a dataset to identify and remove non-relevant factors. The input library type (TuDstd or TuDtail) was set as the factor variable. Following this adjustment, all imputed fold change values were removed.

After combining datasets, differential TuD abundance following repopulation was determined using Wilcoxon's rank-sum test. P-values were calculated for each TuD in comparison to the population of control TuD replicates (i.e. TuDs with a control MBS1 paired with a control MBS2; n=99). To correct for multiple testing, frequentist q-values (FDR) were derived from rank sum p-values using the 'qqvalue' Stata package [40] according to the Benjamini–Hochberg step-up procedure. [41] TuDs with an FDR<0.05 were defined as significantly altered following repopulation.

Bradley-Terry modeling

To perform Bradley-Terry modeling, we first tallied wins and losses for each ordered MBS pairing across all replicates by comparing the MBS1 and MBS2 strength scores. A win was assigned to the MBS with the higher strength score; a loss was assigned to the MBS with lower strength score. The Bradley-Terry model of pairwise comparisons was then applied to win and loss tallies across the entire

data set using the BradleyTerry2 package for R. [42] The scramble-1 MBS was used as the model reference.

MBS phenotypes

For each MBS, we assigned a 'phenotype,' defined as the median standardized $\log_2$ fold change of all TuDs containing the MBS paired with a control (non-targeting) MBS among all replicates of the integrated data set. Each MBS phenotype is therefore derived from up to 72 fold change values (6 control MBSs x 2 orientations x 6 liver replicates). Three MBSs (scramble-3, miR-1a-1-5p, and miR-126-5p) had fewer than 20 such pairings, thus were not assigned a phenotype, and were excluded from further analyses.

Strength scores

For each detected TuD within each liver sample, a strength score was assigned to its constituent MBSs. The strength score of an MBS was defined as the ratio of the distance between the MBS phenotypes of both constituent MBSs ($|MBS1_{phenotype} - MBS2_{phenotype}|$) and the distance of the MBS phenotype to the TuD $\log_2$ fold change ('observed phenotype'):

$$\text{MBS1 strength score} = |MBS1_{phenotype} - MBS2_{phenotype}| \,/\, |MBS1_{phenotype} - \text{observed phenotype}|$$

$$\text{MBS2 strength score} = |MBS1_{phenotype} - MBS2_{phenotype}| \,/\, |MBS2_{phenotype} - \text{observed phenotype}|$$

For each MBS, overall strength scores were defined as the median strength score of the MBS across all TuDs containing the MBS.

MicroRNA interaction (MI) scores

Under the multiplicative model of pairwise genetic interaction between gene A and B, the interaction ($AB_{interaction}$) is defined as the difference between the observed phenotype ($AB_{observed}$) and the predicted AB phenotype ($AB_{predicted}$):

$$AB_{interaction} = AB_{observed} - AB_{predicted}$$

where ($AB_{predicted}$) is the product of the observed individual gene phenotypes:

$$AB_{predicted} = A_{phenotype} \times B_{phenotype}$$

As our MBS phenotypes are defined on the log2 scale, the predicted TuD phenotype ($TuD_{predicted}$) is:

$$TuD_{predicted} = MBS1_{phenotype} + MBS2_{phenotype}$$

For each TuD, we assigned a raw miRNA interaction (MI_{raw}) score equal to its residual from a LOWESS line fitted to the observed phenotype versus $TuD_{predicted}$ scatterplot. Modified t-value (MI_T) scores [26] were then calculated for each MBS pairing as described previously for a pairwise CRISPR screen: [36]

$$MI_T = (TuD_{exp} - TuD_{ctrl}) / \sqrt{(S_{var} \div TuD_{exp}N + S_{var} \div TuD_{ctrl}N)}$$

Where:

$$S_{var} = TuD_{exp}V \times (TuD_{exp}N - 1) + TuD_{ctrl}V \times (TuD_{ctrl}N - 1) \div (TuD_{exp}N + TuD_{ctrl}N - 2)$$

TuD_{exp}: the median MI_{raw} score across all replicates for the MBS pairing in either orientation (5'-AB-3' or 5'-BA-3')

$TuD_{exp}N$: the number of MI_{raw} scores for the MBS pairing

$TuD_{exp}V$: the variance of MI_{raw} scores for the MBS pairing

TuD_{ctrl}: the median MI_{raw} score for all control TuDs (containing two control MBSs) across all replicates

$TuD_{ctrl}N$: the number of MI_{raw} scores for all control TuDs

$TuD_{ctrl}V$: the variance of MI_{raw} scores for all control TuDs

Pairwise TuD MI_T scores that were derived from a minimum of six replicates (of a possible 12: 6 animal replicates x 2 possible MBS orientations) and were at least two standard deviations above or below the MI_T score population mean were considered significant miRNA interactions.

_k_-means clustering

To partition hepatocyte transcripts according to expression level during repopulation, we utilized FPKM values from our recently published TRAP-Seq data set. [2] For each transcript, we calculated the proportion of reads (corrected for sample size) derived from three conditions: quiescent, and one and four weeks following the induction of repopulation. *k*-means clustering of read proportions was then performed for transcripts with FPKM>1 using Euclidean distance as the similarity measure. The optimal

number of clusters (4) was determined using the Calinski-Harabasz pseudo-F. To assess GC content, clustered transcripts were aligned to the RefSeq annotations for NCBI37/mm9 using BEDTools v2.25.0. Statistical significance of differences in GC content between clusters was determined using the Kolmogorov-Smirnov test.

Pathway and motif enrichment

Sets of mRNAs were subjected to gene ontology (categories: Biological Process, Cellular Component, Molecular Function) overrepresentation enrichment analysis using WebGestalt 2017. [43] Significant overrepresentation was defined by a Benjamini-Hochberg corrected FDR<0.05. Overrepresentation analysis of miRNA target site enrichment in TRAP-Seq clusters was performed using the MSigDB v6.0 miRNA network on WebGestalt 2017. Transcripts with less than one FPKM across all samples were excluded from the analysis. For presentation purposes, the list of significantly overrepresented miRNA binding sites was filtered to include only miRNAs tested in our screens. Enriched transcription factor binding motifs within sets of significantly altered genes from the TuD TRAP-Seq experiment were identified using the iRegulon plugin, v1.3 for Cytoscape. [28]

MicroRNA target prediction

Mouse mRNA 3'UTRs containing miR-374b-5p seed sequences were retrieved from SeedBank v1.1 on the seedViscious web server. [44] Transcripts predicted to be targeted by specific families of miRNAs were identified using mirPath v.3. [45] Gene browser tracks of miRNA binding sites were generated for microT-CDS predictions using the DIANA Web Server v5.0. [46]

Human liver cancer data set

MEX3C expression data from The Cancer Genome Atlas (TCGA) was accessed and visualized using the UCSC Xena platform (doi: https://doi.org/10.1101/326470).

Statistical analyses and data visualization

For *in vitro* luciferase assays, treatment groups were compared by repeated measures ANOVA with Dunnet's test for multiple comparisons using Prism 6 (GraphPad Software). All other statistical

analyses were performed using Stata software (StataCorp). Significance of gene or TuD set intersections was determined using a one-tailed Fisher's exact (hypergeometric) test. Similarity of hierarchical cluster MBS membership by MBS position (MBS1 or MBS2) on the TuD $\log_2$ fold change heatmap was determined by Pearson's χ^2 test. Differences in proportion of mRNAs containing a miR-374b-5p seed sequence were assessed using a two-sample proportion test. Differences in distributions were compared using the Kolmogorov-Smirnov test for equality of distribution functions. Statistical tests presented within figures are presented in Supplementary Table 4.

Mancala plots were developed to visualize MBS win and loss tallies used in Bradley-Terry modeling. The Mancala plot is a scatter plot of MBS1 and MBS2 win and loss tallies for each TuD. Data points are jittered to reveal density at the bins. The plot is rotated 45 degrees such that the victory margin becomes the vertical axis. Hive plots were produced using jhive v0.2.7.[47] Hierarchical cluster analyses with Ward's linkage were performed using the heatmap.2 function from the gplots package for R.[48] Remaining heatmaps were generated using the matrix2png web interface.[49] The arc diagram of TuD RNA secondary structure was derived using the R-chie web server.[50] All other plots were derived using Stata software (StataCorp).

SUPPLEMENTARY FIGURE LEGENDS

Supplementary Figure 1. Sequential ligation of MBS pools for the generation of large TuD libraries. (A) A ssRNA tough decoy (TuD) containing two microRNA-binding sites (MBSs). (B) Schematic of the MBS cloning site of pBT264-MBSacceptor. The arc diagram displays the expected secondary structure of the TuD RNA formed by the stem and loop sequences shared across all TuDs, independent of the variable MBS sequences.

Supplementary Figure 2. Both TuD libraries enable repopulation of *Fah*$^{-/-}$ livers through clonal expansion of transfected hepatocytes. (A) Mouse body weights over the four-week repopulation time course. (B) Representative correlations of plasmid input replicates. (C) Mouse liver replicate

correlations of TuDstd (top panel) and TuDtail (bottom panel) experiments. (D) Scatterplots of the first two eigenvectors (components) derived by principal component analyses performed independently for each experiment. Data points are colored according to sample type (liver, purple; plasmid, lime). Axes have been sized relative to the component eigenvalues.

Supplementary Figure 3. Analysis of high-throughput sequencing data following liver repopulation. (A) Volcano plots of TuDstd and TuDtail experiments following DESeq2 analysis. Significantly altered TuDs are colored according to depletion (blue) or enrichment (orange). Histograms of TuD fold change (log_2) and Wilcoxon ranksum p-value (log_{10}) distributions are displayed along the axes. (B) Scatter plot comparing log_2 fold change distributions of TuDstd and TuDtail experiments. Colored data points indicate TuDs with an adjusted $P<.05$. (C) Upset plot of the overlap of significantly altered TuD sets between TuDstd and TuDtail experiments. ***$P<.001$. (D) Combination of TuDstd and TuDtail datasets using internal negative control TuDs. Heatmap of Spearman's rank correlation coefficient values between liver replicates before (left) and after (right) Removal of Unwanted Variation (RUV) data transformation. (E) Representative scatter plots of TuD log_2 fold change values of liver replicates before (left) and after (right) data transformation. ρ, Spearman's rank correlation coefficient. (F) Volcano plot of combined TuD datasets after RUV transformation. Significantly altered TuDs were identified by comparison to negative control TuDs. Colored data points indicate enriched (orange) or depleted (blue) TuDs with an FDR<0.05. Statistical significance was determined using the Wilcoxon rank-sum test with Benjamini-Hochberg multiple tests correction.

Supplementary Figure 4. TuD effects are largely independent of MBS orientation. (A) Dendrograms and heatmap of log_2 fold changes of the combined datasets. Colored bars indicate cluster annotations; black, missing values. (B) Overlap of the MBS clusters annotated in the log_2 fold change heatmap of panel A. Lines connect each MBS according to position (MBS1 or MBS2). MBSs that appear in the same cluster regardless of TuD position are connected by a colored line. Those MBSs with disjoint clustering across position are connected by a gray line. (C) Scatterplot of transformed log_2 fold changes

for TuD pairs where the constituent MBSs A,B are in opposite orientations. MBS combinations that were significantly altered in both orientations are colored according to agreement (orange, blue) or disagreement (red). □, Spearman's rank correlation coefficient. (D) Overlap of significant TuD sets according to MBS orientation. Set comparisons are indicated by colored circles. The top bar chart displays the expected and observed overlap between sets. All observed set overlaps were significantly different than expected by chance. Hypergeometric test: **P*=.018, ****P*<.001. (E) Hive plots displaying the position occupied by the indicated MBS in all significantly altered TuDs (orange, blue). Colored points indicated MBS combinations for which both orientations were significantly altered (FDR<0.05). The vertical axis indicates the partner MBS and is ordered as in Supplementary Table 1.

Supplementary Figure 5. Scoring miRNA inhibition effects by phenotype and strength metrics (A) Quantile plot of 174 individual MBS phenotypes defined as the median transformed $\log_2$ fold change of each MBS when paired with a control MBS. MBSs with the highest (orange) and lowest (blue) phenotypes are indicated on the accompanying rug plot (right panel). Control MBS phenotypes are shown in red. Vertical bars indicate 95% confidence interval estimations. (B) Derivation of MBS strength scores. (C) MBS strength scores were significantly correlated with MBS phenotypes. Scores were regressed on the phenotype and the square of the phenotype. Control MBSs are displayed in red.

Supplementary Figure 6. Scoring miRNA inhibition effects on liver repopulation using Bradley-Terry probability modeling. (A) For each pairwise TuD within each sample, the two constituent MBSs were assigned a win or loss based on MBS phenotypes and the observed TuD $\log_2$ fold change. Wins and losses were tallied for each ordered pairing across all replicates and used as the input for a Bradley-Terry model of pairwise comparisons. (B) Quantile plot of Bradley-Terry model coefficients for 174 individual MBSs. The top three MBSs by coefficient are colored by enriched (orange) or depleted (blue) phenotypes. Control MBS coefficients are shown in red. (C Bradley-Terry model coefficients were significantly correlated with MBS strength scores. □, Spearman's correlation coefficient. (D) Mancala

plots of win and loss tallies for all TuDs containing a miR-374b-5p MBS (left panel) or miR-539-5p (right panel).

Supplementary Figure 7. Putative target pathways overlap (A) Heatmap displaying the KEGG pathways significantly enriched for the miRNAs indicated, as predicted by microT-CDS. (B) KEGG pathways enriched for predicted targets of the 11 members of the miR-10a/miR-30 families displayed in Figure 4.

Supplementary Figure 8. Repopulating hepatocytes increase expression of AU-rich transcripts and miR-374b-5p. (A) Kernel density plot of mRNA GC content. Dashed vertical lines indicate population medians. Densities were compared using a two-sample Kolmogorov-Smirnov test. (B) AGO2-bound miR-374b-5p levels increase in mice following partial hepatectomy.[3] (C) The miR-374b host gene, *Ftx*, showed increased chromatin accessibility at the promoter during liver repopulation in *Fah*$^{-/-}$ mice.[2]

Supplementary Figure 9. Profiling miR-374b-5p effects by translating ribosome affinity purification followed by RNA sequencing. (A) Body weights of mice injected with TRAP-Seq plasmids expressing TuDs containing a miR-880-5p MBS paired with a scramble-3 MBS (green) or with a miR-374b-5p MBS (pink). Data are presented as mean ± 95% confidence intervals with smoothed fit lines. (B) Heatmap of significantly altered transcripts encoding subunits of the cytosolic ribosome. (C) The ribosome subunit transcripts of panel B plotted as a fraction of FPKM from our previous TRAP-Seq data set.[2] (D) *Igf2* and *Afp* mRNAs display reduced ribosomal occupancy in TuD374 treated mice, consistent with accelerated repopulation. Values are displayed as transcripts per kilobase million (TPM). (E) Motif analysis of genes up- or down-regulated by TuD374 within +/-20 kilobase of the TSS. Left panel, transcription factors (TF) associated with the top four motif clusters by normalized expression score (NES) within each gene set. Right panel, quantile plots of enriched motif NES. Colored data points indicate enriched motifs for the indicated motif cluster. Sequence logos of the top motifs are shown as insets.

Supplementary Table 1. MicroRNA-binding site sequences.
The table below lists the microRNA-binding site (MBS) RNA sequences. The DNA oligonucleotide sequences for insertion into pBT264-MBSacceptor are derived as follows:

(1) Convert the RNA sequence below to DNA ('top strand')
(2) Derive the reverse complement DNA sequence ('bottom strand')
(3) To the 5' end of the top strand, add 'CTTC'"
(4) To the 5' end of the bottom strand, add 'CGGT'"

MBS	Sequence (5' -> 3')
let-7a-3p	GGAAAGACAGUCAAAAGAUUGUAUAG
let-7a-5p	AACUAUACAACAAACCUACUACCUCA
let-7b-3p	GGGAAGGCAGUCAAAAGGUUGUAUAG
let-7b-5p	AACCACACAACAAACCUACUACCUCA
let-7c-5p	AACCAUACAACAAACCUACUACCUCA
let-7d-3p	AGAAAGGCAGCAAAAAGGUCGUAUAG
let-7d-5p	AACUAUGCAACAAACCUACUACCUCU
let-7e-5p	AACUAUACAACAAACCUCCUACCUCA
let-7f-3p	GAAAGACAGUACAAAGACUGUAUAG
let-7f-5p	AACUAUACAAUCAACCUACUACCUCA
let-7g-5p	AACUGUACAAACAACCUACUACCUCA
let-7i-3p	AGCAAGGCAGUCAAAAGCUUGCGCAG
let-7i-5p	AACAGCACAAACAACCUACUACCUCA
miR-100-5p	CACAAGUUCGGAAACAUCUACGGGUU
miR-101a-3p	UUCAGUUAUCACAACCAGUACUGUA
miR-101a-5p	GCAUCAGCACUCAACGUGAUAACUGA
miR-101b-3p	AGCUAUCACACAAAGUACUGUAC
miR-101c	UCAGUUAUCACAACCAGUACUGU
miR-103-1-3p	UCAUAGCCCUGUCAACACAAUGCUGCU
miR-106b-3p	GCAGCAAGUACAAAACCACAGUGCGG
miR-107-3p	UGAUAGCCCUGUCAACACAAUGCUGCU
miR-10a-5p	CACAAAUUCGGACAACUCUACAGGGUA
miR-122-3p	UUAGUGUGAUCAACAAUGGCGUUU
miR-122-5p	CAAACACCAUUCAACGUCACACUCCA
miR-125a-3p	GGCUCCCAAGACAACACCUCACCUGU
miR-125a-5p	UCACAGGUUAAACAACGGGUCUCAGGGA
miR-125b-1-5p	UCACAAGUUAGAAACGGUCUCAGGGA
miR-125b-2-3p	AGGUCCCAAGACAACACCUGACUUGU
miR-126-3p	CGCAUUAUUACAAACUCACGGUACGA
miR-126-5p	CGCGUACCAAACAAAAGUAAUAAUG
miR-130b-3p	AUGCCCUUUCACAAAUCAUUGCACUG
miR-136-5p	CCAUCAUCAAACAACACAAAUGGAGU
miR-140-3p	CCGUGGUUCUACAACCCCUGUGGUA

miR-140-5p	CUACCAUAGGGAAAAUAAAACCACUG
miR-142-3p	UCCAUAAAGUAGAAACGAAACACUACA
miR-142-5p	AGUAGUGCUUUCAAACUACUUUAUG
miR-143-3p	GAGCUACAGUGAAACCUUCAUCUCA
miR-143-5p	CCAGAGAUGCACAAAGCACUGCACC
miR-144-3p	AGUACAUCAUCAACCUAUACUGUA
miR-144-5p	ACUUACAGUAUACAAAUGAUGAUAUCC
miR-145-5p	AGGGAUUCCUGGAAAAGAAAACUGGAC
miR-146a-5p	AACCCAUGGAACAACUUCAGUUCUCA
miR-146b-5p	AGCCUAUGGAACAACUUCAGUUCUCA
miR-148a-3p	ACAAAGUUCUGAAACUAGUGCACUGA
miR-151-3p	CCUCAAGGAGCAAAACUCAGUCUAG
miR-151-5p	ACUAGACUGUGAAACAGCUCCUCGA
miR-152-3p	CCAAGUUCUGUCAACCAUGCACUGA
miR-15a-5p	CACAAACCAUUCAACAUGUGCUGCUA
miR-15b-3p	UAGAGCAGCAACAAAAUAAUGAUUCG
miR-16-1-3p	UCAGCAGCACACAAAGUCAAUACUGG
miR-16-1-5p	CGCCAAUAUUUCAACACGUGCUGCUA
miR-16-2-3p	AAAGCAGCACACAACAUAAUAUUGGU
miR-17-5p	CUACCUGCACUGAAAAUAAGCACUUUG
miR-181b-2-5p	ACCCACCGACAGAAACCAAUGAAUGUU
miR-181c-5p	ACUCACCGACACAACGGUUGAAUGUU
miR-1839-5p	CAAGACCUGUUCAACCUAUCUACCUU
miR-1843-5p	AGUCAGACAGACAACGACCUCCAUA
miR-1843b-5p	AAGUCAGACAGAAACAGACCUCCAU
miR-185-5p	UCAGGAACUGCAAACCUUUCUCUCCA
miR-186-5p	AGCCCAAAAGGAAAAAGAAUUCUUUG
miR-188-5p	CCCUCCACCAUCAAAGCAAGGGAUG
miR-190-5p	ACCUAAUAUAUCAACCAAACAUAUCA
miR-192-3p	CUGUGACCUAUCAAAGGAAUUGGCAG
miR-192-5p	GGCUGUCAAUUCAAACAUAGGUCAG
miR-193-3p	ACUGGGACUUUCAACGUAGGCCAGUU
miR-193b-3p	AGCGGGACUUUCAACGUGGGCCAGUU
miR-194-1-5p	UCCACAUGGAGAAACUUGCUGUUACA
miR-194-2-3p	CAGAUAACAGCAAAAAGCCCCACUGG
miR-1948-5p	AUUUAGGCAGACAACAUACUCAUAU
miR-195-5p	GCCAAUAUUUCAAACUGUGCUGCUA
miR-1981-5p	GCCACGUCUAAGAAAACCCAGCCUUUAC
miR-200b-3p	UCAUCAUUACCAAACAGGCAGUAUUA
miR-203-3p	CUAGUGGUCCUCAAAAAACAUUUCAC
miR-20a-5p	CUACCUGCACUACAACUAAGCACUUUA
miR-20b-5p	CUACCUGCACUACAAAUGAGCACUUUG

miR-21-3p	GACAGCCCAUCAAAAGACUGCUGUUG
miR-21-5p	UCAACAUCAGUCAACCUGAUAAGCUA
miR-210-3p	UCAGCCGCUGUCAAACACACGCACAG
miR-214-3p	ACUGCCUGUCUCAACGUGCCUGCUGU
miR-215-5p	GUCUGUCAAAUCAACCAUAGGUCAU
miR-22-3p	ACAGUUCUUCACAACACUGGCAGCUU
miR-221-3p	GAAACCCAGCAGAAACACAAUGUAGCU
miR-222-3p	ACCCAGUAGCCAAACAGAUGUAGCU
miR-223-3p	UGGGGUAUUUGAAACACAAACUGACA
miR-23a-3p	GGAAAUCCCUGAAACGCAAUGUGAU
miR-23b-3p	GGUAAUCCCUGAAACGCAAUGUGAU
miR-24-1-5p	ACUGAUAUCAGCAAAAUCAGUAGGCAC
miR-24-2-5p	ACUGUUUCAGCAAAAUCAGUAGGCAC
miR-25-3p	UCAGACCGAGACAAACAAGUGCAAUG
miR-26a-1-5p	AGCCUAUCCUGAAACGAUUACUUGAA
miR-26b-3p	GAGCCAAGUAACAAAUGGAGAACAGG
miR-26b-5p	ACCUAUCCUGACAACAUUACUUGAA
miR-27a-3p	GCGGAACUUAGAAACCCACUGUGAA
miR-27b-3p	GCAGAACUUAGAAACCCACUGUGAA
miR-27b-5p	GUUCACCAAUCAAACAGCUAAGCUCU
miR-28-3p	UCCAGCAGCUCAAAAACAAUCUAGUG
miR-28-5p	CUCAAUAGACUCAACGUGAGCUCCUU
miR-297a-1-5p	ACAUGCACAUGAAACCACACAUACAU
miR-29a-3p	UAACCGAUUUCAAACAGAUGGUGCUA
miR-29a-5p	CUGAACACCAACAACAAGAAAUCAGU
miR-29b-2-3p	AACACUGAUUUCAAACAAAUGGUGCUA
miR-301a-3p	GCUUUGACAAUACAAACUAUUGCACUG
miR-3068-3p	UGUUGGAGUACAAAAUGCAAUUCACC
miR-3082-5p	ACACAGACACACAAACACACUCUGUC
miR-30a-5p	CUUCCAGUCGAGAACGGAUGUUUACA
miR-30b-5p	AGCUGAGUGUACAACGGAUGUUUACA
miR-30c-1-5p	GCUGAGAGUGUACAACGGAUGUUUACA
miR-30d-3p	GCAGCAAACAUCAAACUGACUGAAAG
miR-30d-5p	CUUCCAGUCGGAAACGGAUGUUUACA
miR-30e-5p	CUUCCAGUCAACAACGGAUGUUUACA
miR-31-5p	CAGCUAUGCCACAACGCAUCUUGCCU
miR-3105-3p	GGAGUGCAAGCAAACUCAUAAGCAGU
miR-322-5p	UCCAAAACAUGAAAAAAUUGCUGCUG
miR-324-3p	AGCAGCACCUCAAAGGGGCAGUGG
miR-328-3p	ACGGAAGGGCACAAAGAGAGGGCCAG
miR-33-3p	GUGAUGCACUGAAAAUGGAAACAUUG
miR-33-5p	UGCAAUGCAACAAAAUACAAUGCAC
miR-330-3p	UCUCUGCAGGCCAAAACUGUGCUUUGC

miR-331-3p	UUCUAGGAUAGAAAAGCCCAGGGGC
miR-338-3p	CAACAAAAUCACAACCUGAUGCUGGA
miR-338-5p	CACUCAGCACCAAACAGGAUAUUGUU
miR-340-5p	AAUCAGUCUCACAACUUGCUUUAUAA
miR-342-5p	CUCAAUCACAGAAACAUAGCACCCCU
miR-345-3p	GUCUCCAGACCAAAACCUAGUUCAGG
miR-345-5p	AAGCACUGGACAAAAUAGGGGUCAGC
miR-34c-5p	GCAAUCAGCUAACAACCUACACUGCCU
miR-350-5p	CCCAAAGCGCAAACAUGCACUUU
miR-351-3p	GUUCCCAGGCGAAAACCUCUUGACC
miR-351-5p	CAGGCUCAAAGGAAACGCUCCUCAGGGA
miR-362-5p	AUUCACACCUAGAAACGUUCCAAGGAUU
miR-369-3p	AAAGAUCAACCAAACAUGUAUUAUU
miR-374-5p	CACUUAGCAGGAAACUUGUAUUAUAU
miR-376a-5p	ACUCAUAGAAGAAAAGAGAAUCUACC
miR-376c-3p	ACGUGAAAUUUCAACCCUCUAUGUU
miR-378-3p	CCUUCUGACUCAAACCAAGUCCAGU
miR-378-5p	ACACAGGACCUCAAAGGAGUCAGGAG
miR-378b	UCUUCUGACUCAAACCAAGUCCAG
miR-421-3p	GCGCCCAAUUAACAACUGUCUGUUGAU
miR-425-3p	GGCGGACACGACAACCAUUCCCGAU
miR-425-5p	UCAACGGGAGUGAAACAUCGUGUCAUU
miR-451	AACUCAGUAAUCAACGGUAACGGUUU
miR-455-3p	GUGUAUAUGCCAAAACGUGGACUGC
miR-467e-5p	ACAUAUACAUGAAACCUCACACUUAU
miR-487b-5p	CGAAGAGGACACAACGGGAUAACCA
miR-497-3p	CUAACACCACACAAAGUGUGGUUUG
miR-497-5p	UACAAACCACACAAAGUGUGCUGCUG
miR-501-5p	UUUCACCCAGGAAACGACAAAGGAUU
miR-503-3p	CCAGGCAGUGGAAAAAAACAAUACUC
miR-5099	GGAGCACCACAAACAUCGAUCUAA
miR-511-3p	AUCCUGUCUUUCAACUGCUACACAUU
miR-532-5p	ACGGUCCUACACAAACUCAAGGCAUG
miR-539-5p	ACACACCAAGGAAAAAUAAUUUCUCC
miR-551b-3p	CUGAAACCAAGAAAAUAUGGGUCGC
miR-5620-3p	GUGAGGCAGGGAAACGGAUGACUGU
miR-574-5p	ACACACUCACACAAACACACACACUCA
miR-652-3p	CACAACCCUAGAAACUGGCGCCAUU
miR-652-5p	GAAUGGCACCCCAAAACUCCUAGGGUUG
miR-671-5p	CUCCAGCCCCUCAAACCAGGGCUUCCU
miR-674-5p	UACACCACUCCAAAACAUCUCAGUGC
miR-690	UUUGGUUGUGACAACGCCUAGCCUUU
miR-708-5p	CCCAGCUAGAUUCAACGUAAGCUCCUU
miR-7a-1-5p	ACAACAAAAUCACAACCUAGUGUUCCA

miR-802-5p	AAGGAUGAAUCAAACUUUGUUACUGA
miR-872-5p	CCUGAACUAACAAACAAGUAACCUU
miR-873-5p	AGGAGACUCACAAAAAAGUUCCUGC
miR-883b-3p	AUACUGAGAGACAACUGUUGCAGUUA
miR-93-3p	CGGGAAGUGCUCAACAGCUCAGCAGU
miR-93-5p	CUACCUGCACGACAAAACAGCACUUUG
miR-98-5p	AACAAUACAACAAACUUACUACCUCA
miR-99a-3p	AGACCCAUAGACAAAAACGAGCUUG
miR-99a-5p	CACAAGAUCGGAAACAUCUACGGGUU
scramble-1	GUGUAACACGUCAACCUAUACGCCCA
scramble-2	GGUUCGUACGUCAACACACUGUUCA
scramble-3	CGGUACGAUCGCAAAAGGCGGGAUAUC
miR-1a-1-5p	UAUGGGCAUAUACAACAAGAAGUAUGU
miR-670-3p	ACACUCCUGAAUGAAACGAUAUGAGGAAA
miR-880-5p	UGACUCAUAUCAAACAAUCUGAGUA

Supplementary Table 2. High coverage of pKT2-FAH-TuD libraries

	TuDstd			TuDtail		
	Plasmid (n=4)	Liver (n=3)	Both	Plasmid (n=4)	Liver (n=3)	Both
TuDs detected (%)	30817 (98.4)	30317 (96.8)	30308 (96.7)	30846 (98.5)	30796 (98.3)	30795 (98.3)
TuDs > threshold reads (%)	N/A	N/A	24213 (77.3)	N/A	N/A	29530 (94.3)
Mean sample reads	9.84×10^6	8.70×10^6	N/A	3.64×10^7	2.22×10^7	N/A

Supplementary Table 3. Oligonucleotide sequences

Oligonucleotides	**Top strand (5'->3')**	**Bottom strand (5'->3')**
TuD stems and spacers	GATCTGTCGACGACGGCGCTA GGATCATCTTCATATGCAGGTA ATCTCGAGAATACCTGCTTATA CCGTATTCTGGTCACAGAATAC TTCAAGTCTTCTATGGATCCTA TGAAGACAAACCGATGATCCTA GCGCCGTCGCGGCCGC	AATTGCGGCCGCGACGGCGCTA GGATCATCGGTTTGTCTTCATAG GATCCATAGAAGACTTGAAGTAT TCTGTGACCAGAATACGGTATAA GCAGGTATTCTCGAGATTACCTG CATATGAAGATGATCCTAGCGCC GTCGTCGACA
pKT2-Fah-U6-sgRNA-SBK repair fragment - TuDstd	ACCGTCGACAAAAGTACTAAAG CGGCCGCGATTTTTTTAGTTTT TTTG	CTAGCAAAAAAACTAAAAAAATC GCGGCCGCTTTAGTACTTTTGTC GAC
pKT2-Fah-U6-sgRNA-SBK repair fragment - TuDtail	ACCGTCGACAAAAGTACTAAAG CGGCCGC	AATTGCGGCCGCTTTAGTACTTT TGTCGAC
miR-192-5p sensor	TCGAGATAAGGCTGTCAACCAT AGGTCAGACACAGGCTGTCAA CCATAGGTCAGTTATGC	GGCCGCATAACTGACCTATGGTT GACAGCCTGTGTCTGACCTATGG TTGACAGCCTTATC
miR-194-5p sensor	TCGAGATAATCCACATGGACTG CTGTTACAACACATCCACATGG ACTGCTGTTACATTATGC	GGCCGCATAATGTAACAGCAGTC CATGTGGATGTGTTGTAACAGCA GTCCATGTGGATTATC
miR-215-5p sensor	TCGAGATAAGTCTGTCAACCAT AGGTCATACACAGTCTGTCAAC CATAGGTCATTTATGC	GGCCGCATAAATGACCTATGGTT GACAGACTGTGTATGACCTATGG TTGACAGACTTATC
Control shRNA	TCTCGCCTAAGGTTAAGTCGCC CTCGCTCGAGCGAGGGCGACT TAACCTTAGGCT	CTGCAGCCTAAGGTTAAGTCGCC CTCGCTCGAGCGAGGGCGACTT AACCTTAGGC
miR-374b hairpin	TCTCGGAAGAAATCCTACTCGG GTGGATATAATACAACCTGCTA AGTGTTCTAGCACTTAGCAGGT TGTATTATCATTGTCCGAGGTT ATGGCTCTCGTCCT	CTGCAGGACGAGAGCCATAACC TCGGACAATGATAATACAACCTG CTAAGTGCTAGAACACTTAGCAG GTTGTATTATATCCACCCGAGTA GGATTTCTTCC
PCR primers	**Forward (5'->3')**	**Reverse (5'->3')**
Illumina First PCR	AATGATACGGCGACCACCGAG ATCTACACTCTTTCCTCGACGA CGGCGCTAGGATCATCTTC	GTGACTGGAGTTCAGACGTGTG CTCTTCCGATCTCAGTGGTATTT GTGAGCCAGGGCATTGGC
Illumina Second PCR	AATGATACGGCGACCACCGAG ATCTACACTCTTTCC	*Illumina index primer*
NheI-U6-TuDacceptor-pT	ATTATTGCTAGCTGAGATGCAG ATCGCAGA	TTGTTTAACTTGGTCTCCCTTTA
Mouse Mex3c 3'UTR	ATTATTCTCGAGAAAGGCATGG GTATAATGGTA	ATTATTGCGGCCGCACATTCAAG TTAATGGAAACAAGT
Mex3c 3'UTR deletion 1		ATTATTGCGGCCGCTGACTTCCC TACATATACATAACAAA
Mex3c 3'UTR deletion 2		ATTATTGCGGCCGCATGTTTCAC ATTTTGAGCTACAG
Sequencing primers	**5'->3'**	**Note**
pBT264-MBSacceptor SeqR	TGAAATTTGTGATGCTATTGCT	Identify MBS inserts in pBT264-MBSacceptor
pKT2-Fah-TuDacceptor SeqR	ATTTCTTTCATCACATTCCCAGT	Identify TuD inserts in pKT2-TuD plasmids

TuD Seq primer	CTCGACGACGGCGCTAGGATC ATCTTC	Custom Illumina sequencing primer

Supplementary Table 4. Statistical tests in figures

Figure	**Test**	**Multiple tests correction**
1C	Repeated measures ANOVA	Dunnet's test
2D	Spearman's rank-order correlation	
3C	Two-sample Kolmogorov-Smirnov	
4B	None; considered plus/minus 2 SD from mean as significant interaction score	
4D	None; considered plus/minus 2 SD from mean as significant interaction score	
4E	None; considered plus/minus 2 SD from mean as significant interaction score	
5B	Hypergeometric	Benjamini-Hochberg
5C	Two-sample Kolmogorov-Smirnov	
6C	Studen't t-test, paired	
6D	Wald test (*DESeq2*)	Benjamini-Hochberg
6E	Hypergeometric	Benjamini-Hochberg
6F	Two-sample test of proportion	
6G	Hypergeometric	
6H	Studen't t-test, paired	
7E	Studen't t-test, paired	
7F	Log-rank test (Xena Browser)	
S3A	Wald test (*DESeq2*)	Benjamini-Hochberg
S3B	Spearman's rank-order correlation	
S3C	Hypergeometric	
S3D	Spearman's rank-order correlation	
S3E	Spearman's rank-order correlation	
S3F	Wilcoxon's rank-sum	Benjamini-Hochberg
S4B	Pearson's chi-squared	
S4C	Spearman's rank-order correlation	
S4D	Hypergeometric	
S6C	Spearman's rank-order correlation	
S7A	Two-sample Kolmogorov-Smirnov	
S8D	Wald test (*DESeq2*)	Benjamini-Hochberg
S8E	NES (iRegulon plugin for Cytoscape)	

S9A	Studen't t-test, paired	

Supplementary Table 5. TuD374/TuDctrl competition sequencing counts

	TuDctrl - Input		TuD374 - Input		TuDctrl – Liver		TuD374 – Liver		TuD374/TuDctrl	
Mouse	Forward	Reverse	Forward	Reverse	Forward	Reverse	Forward	Reverse	Input	Liver
1	4281	4515	2105	2245	4485	4800	3406	3677	0.494	0.763
2	4062	4291	1902	2037	6214	6551	4647	4961	0.471	0.753
3	5711	6072	2986	3178	5091	5445	3376	3576	0.523	0.660
4	5318	5641	2804	3009	5045	5384	3644	3908	0.530	0.724
5	8289	8763	4336	4610	5727	6053	3882	4137	0.525	0.681
6	8287	8773	3462	3690	4359	4610	3471	3708	0.419	0.800
7	6239	6650	3522	3798	4456	4731	2388	2541	0.568	0.537

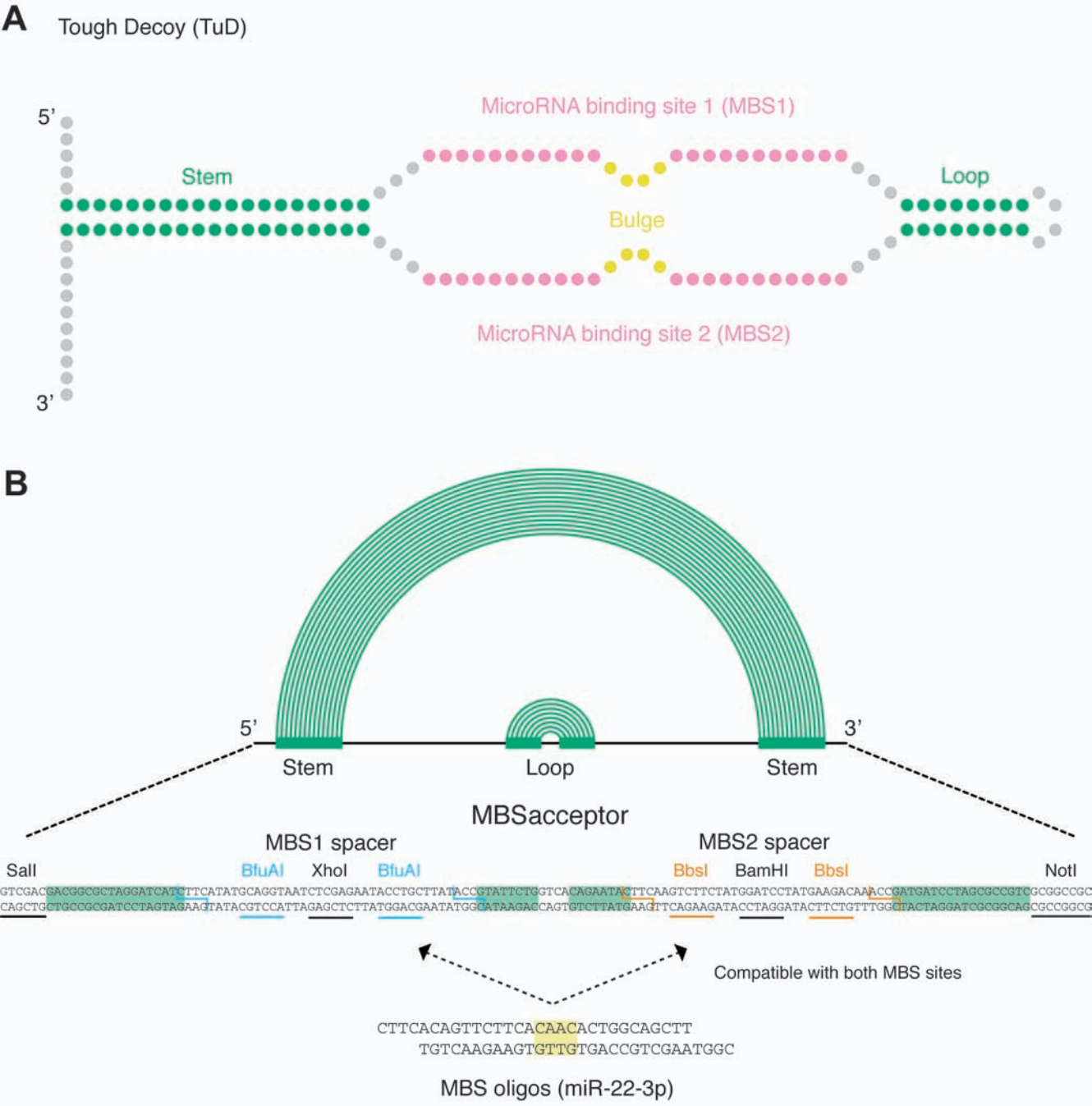
A
Tough Decoy (TuD)
5'
3'
Stem
MicroRNA binding site 1 (MBS1)
Bulge
Loop
MicroRNA binding site 2 (MBS2)
B
5'
3'
Stem
Loop
Stem
MBSacceptor
MBS1 spacer
MBS2 spacer
SalI
BfuAI
XhoI
BfuAI
BbsI
BamHI
BbsI
NotI
GTCGACGACGGCGCTAGGATCATCTTCATATGCAGGTAATCTCGAGAATACCTGCTTATACCGTATTCTGGTCACAGAATACTTCAAGTCTTCTATGGATCCTATGAAGACAAACCGATGATCCTAGCGCCGTCGCGGCCGC
CAGCTGCTGCCGCGATCCTAGTAGAAGTATACGTCCATTAGAGCTCTTATGGACGAATATGGCATAAGACCAGTGTCTTATGAAGTTCAGAAGATACCTAGGATACTTCTGTTTGGCTACTAGGATCGCGGCAGCGCCGGCG
Compatible with both MBS sites
CTTCACAGTTCTTCACAACACTGGCAGCTT
TGTCAAGAAGTGTTGTGACCGTCGAATGGC
MBS oligos (miR-22-3p)

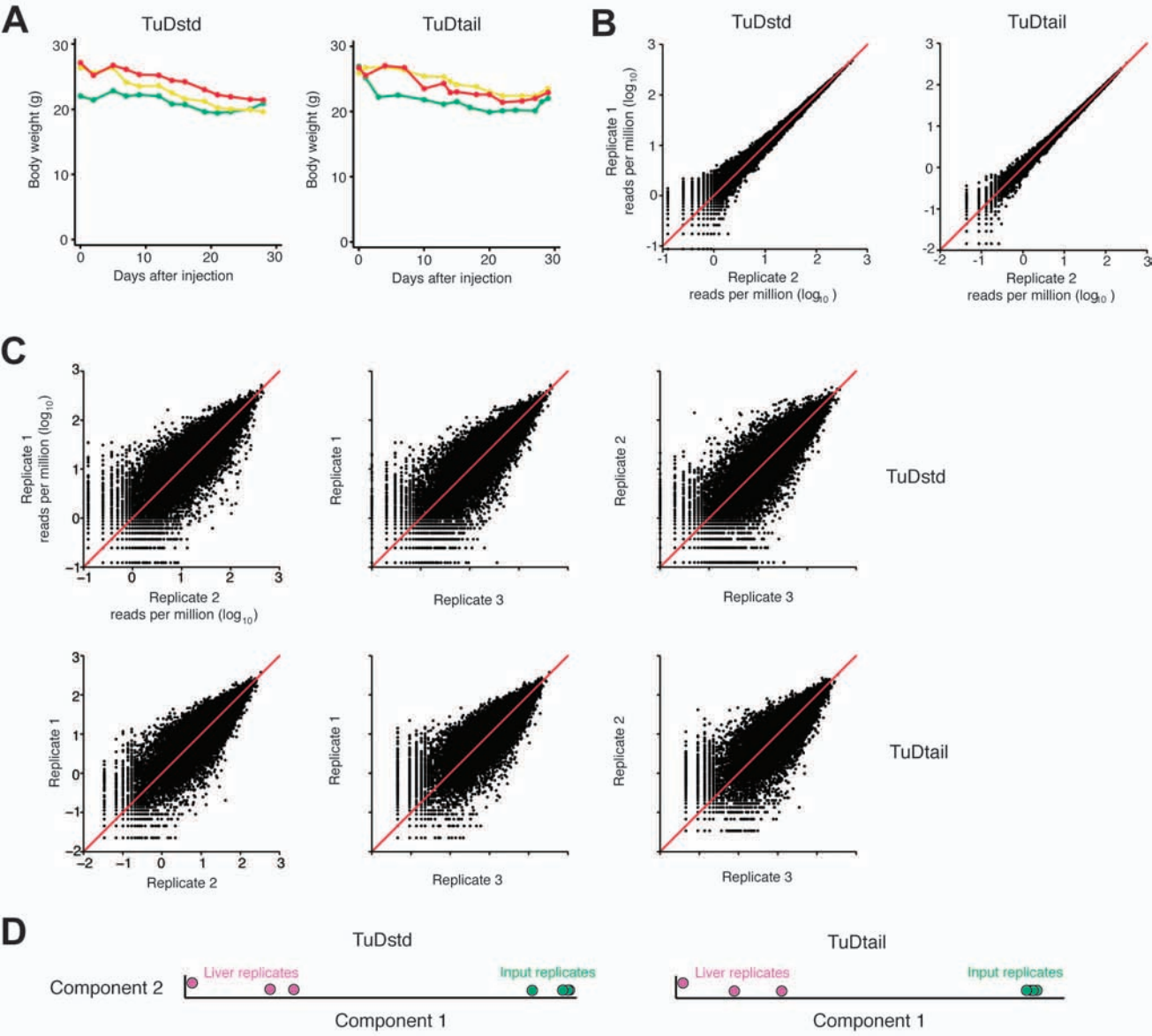
A
TuDstd
TuDtail
Body weight (g)
Days after injection
B
TuDstd
TuDtail
Replicate 1
reads per million (log10)
Replicate 2
reads per million (log10)
C
TuDstd
TuDtail
Replicate 1
Replicate 2
Replicate 3
D
TuDstd
TuDtail
Component 2
Component 1
Liver replicates
Input replicates

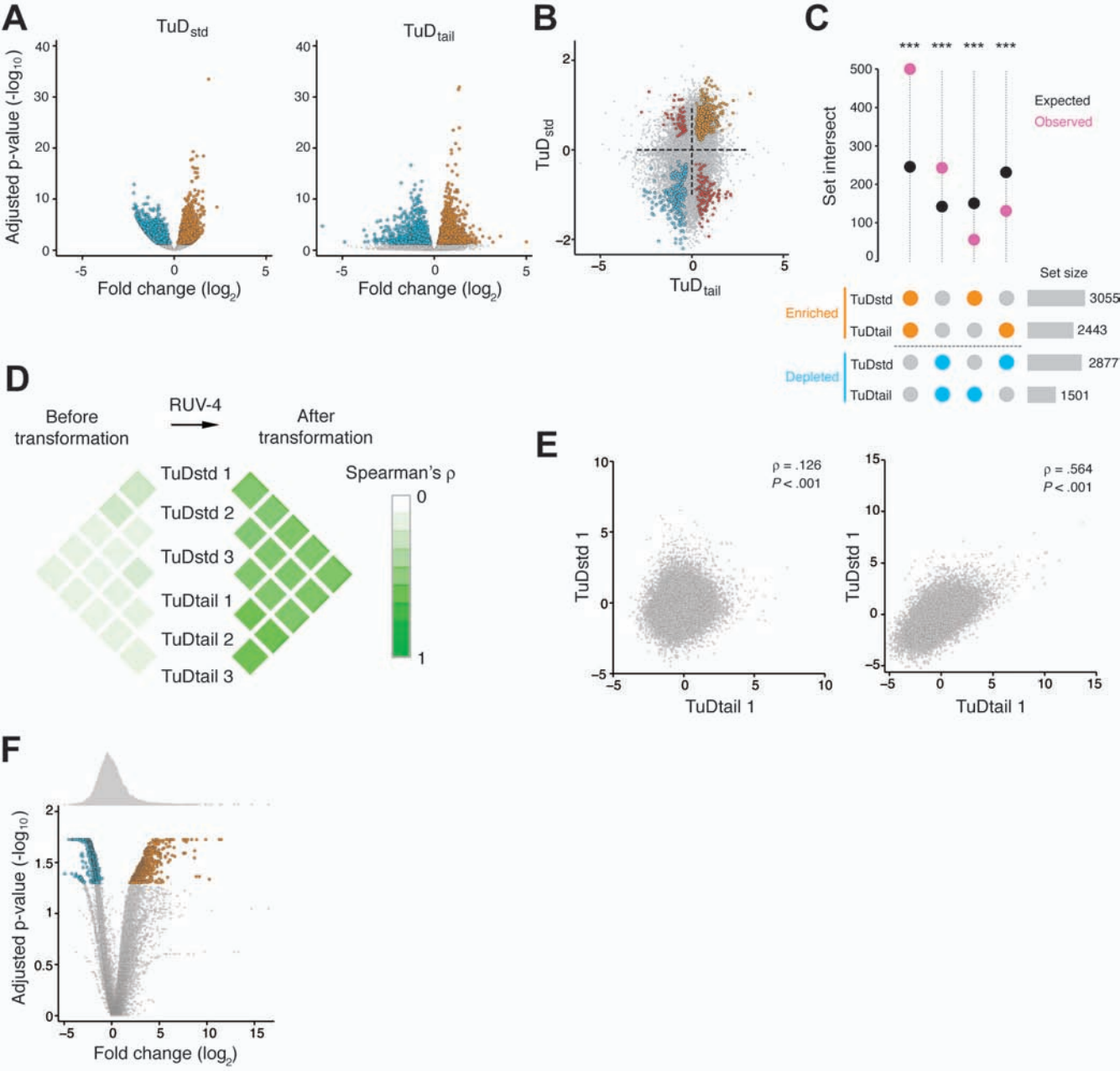
A
TuDstd
TuDtail
Adjusted p-value (-log10)
Fold change (log2)
B
TuDstd
TuDtail
C
***
Set intersect
Expected
Observed
Set size
Enriched
TuDstd
TuDtail
3055
2443
Depleted
TuDstd
TuDtail
2877
1501
D
Before transformation
RUV-4
After transformation
TuDstd 1
TuDstd 2
TuDstd 3
TuDtail 1
TuDtail 2
TuDtail 3
Spearman's ρ
0
1
E
ρ = .126
P < .001
ρ = .564
P < .001
TuDstd 1
TuDtail 1
F
Adjusted p-value (-log10)
Fold change (log2)

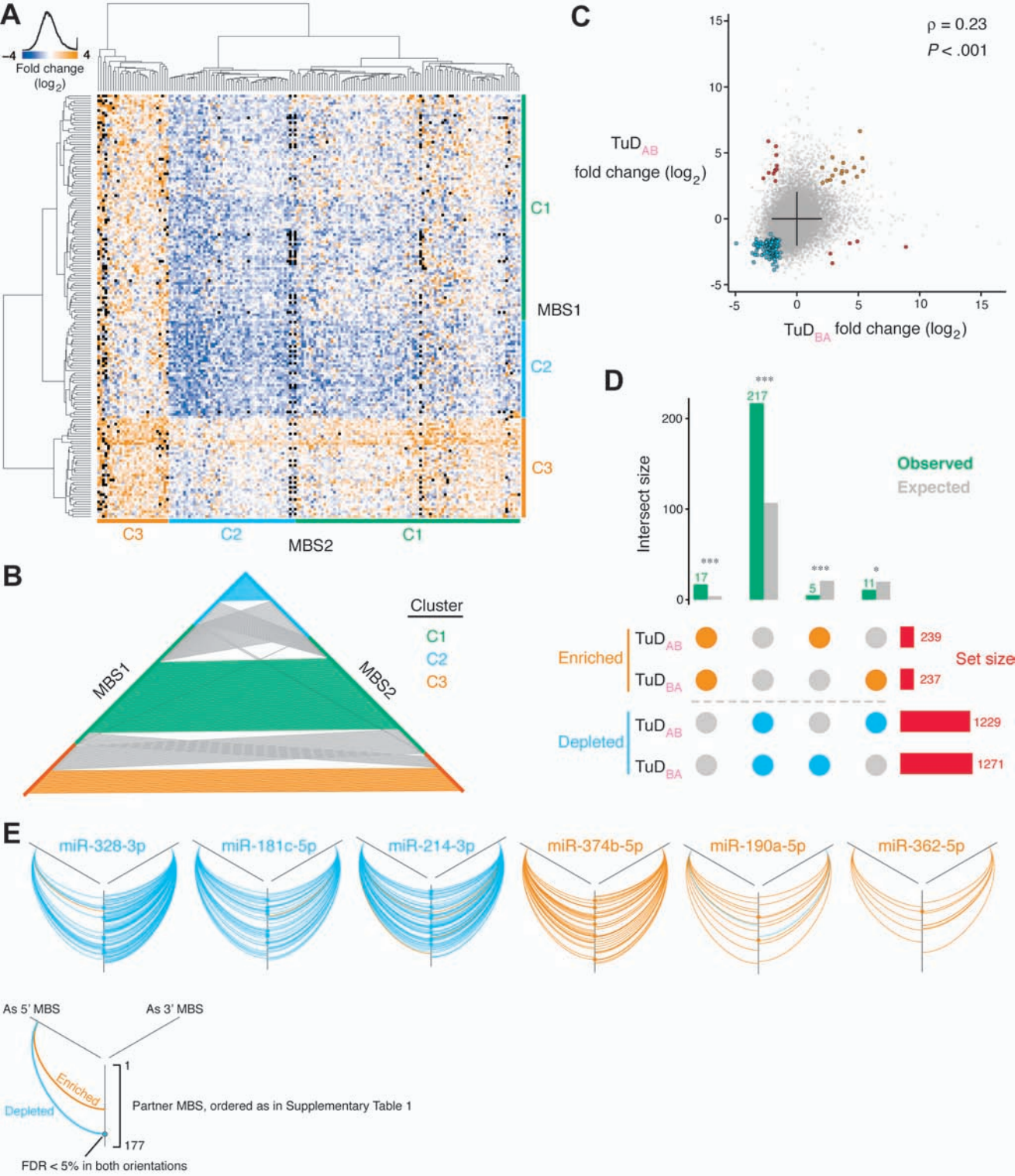
A
−4
4
Fold change
(log2)
C1
MBS1
C2
C3
C3
C2
C1
MBS2
B
Cluster
C1
C2
C3
MBS1
MBS2
C
ρ = 0.23
P < .001
TuDAB
fold change (log2)
TuDBA fold change (log2)
D
Intersect size
Observed
Expected
***
217
***
***
*
17
5
11
Enriched
TuDAB
TuDBA
Depleted
TuDAB
TuDBA
239
237
1229
1271
Set size
E
miR-328-3p
miR-181c-5p
miR-214-3p
miR-374b-5p
miR-190a-5p
miR-362-5p
As 5' MBS
As 3' MBS
Enriched
Depleted
1
177
Partner MBS, ordered as in Supplementary Table 1
FDR < 5% in both orientations

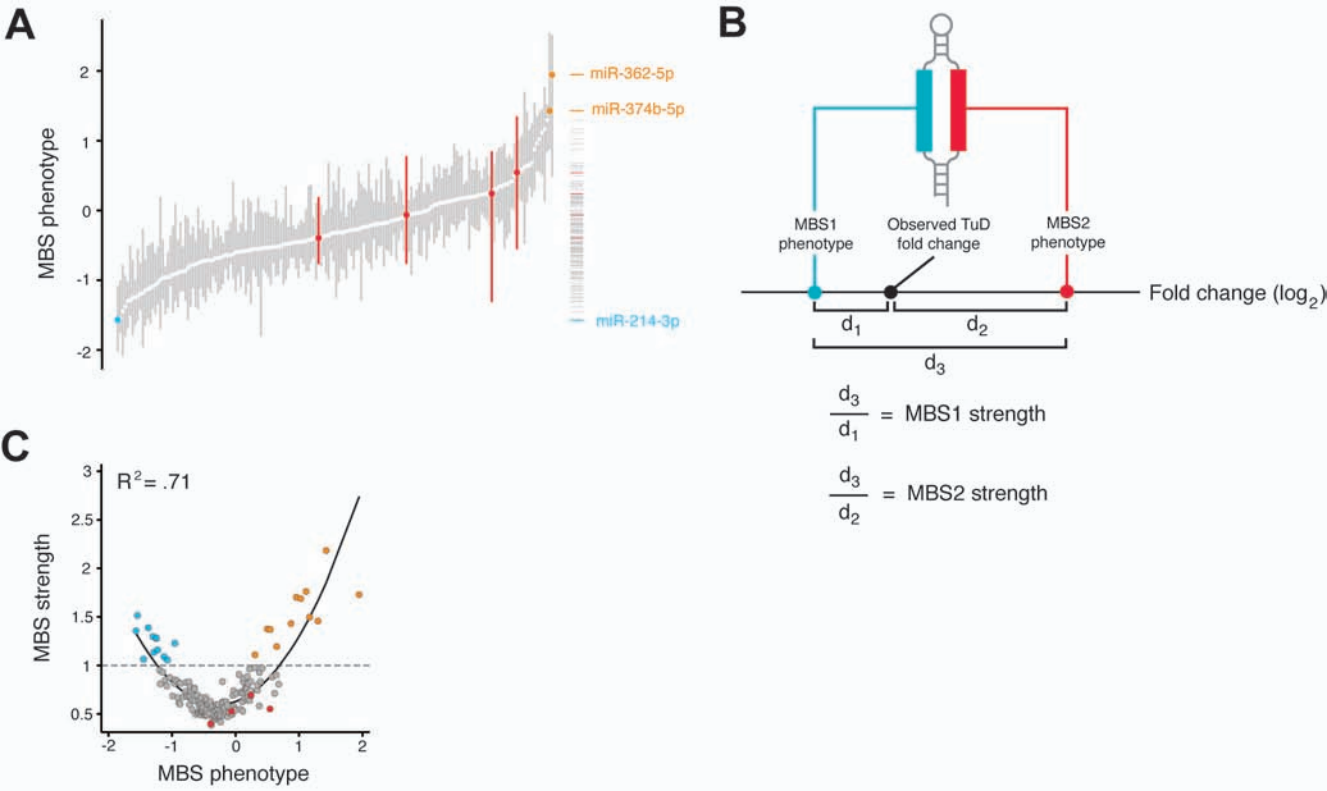
A
MBS phenotype
2
1
0
-1
-2
miR-362-5p
miR-374b-5p
miR-214-3p
B
MBS1
phenotype
Observed TuD
fold change
MBS2
phenotype
Fold change (log2)
d1
d2
d3
d3/d1 = MBS1 strength
d3/d2 = MBS2 strength
C
R2= .71
MBS strength
3
2.5
2
1.5
1
0.5
-2
-1
0
1
2
MBS phenotype

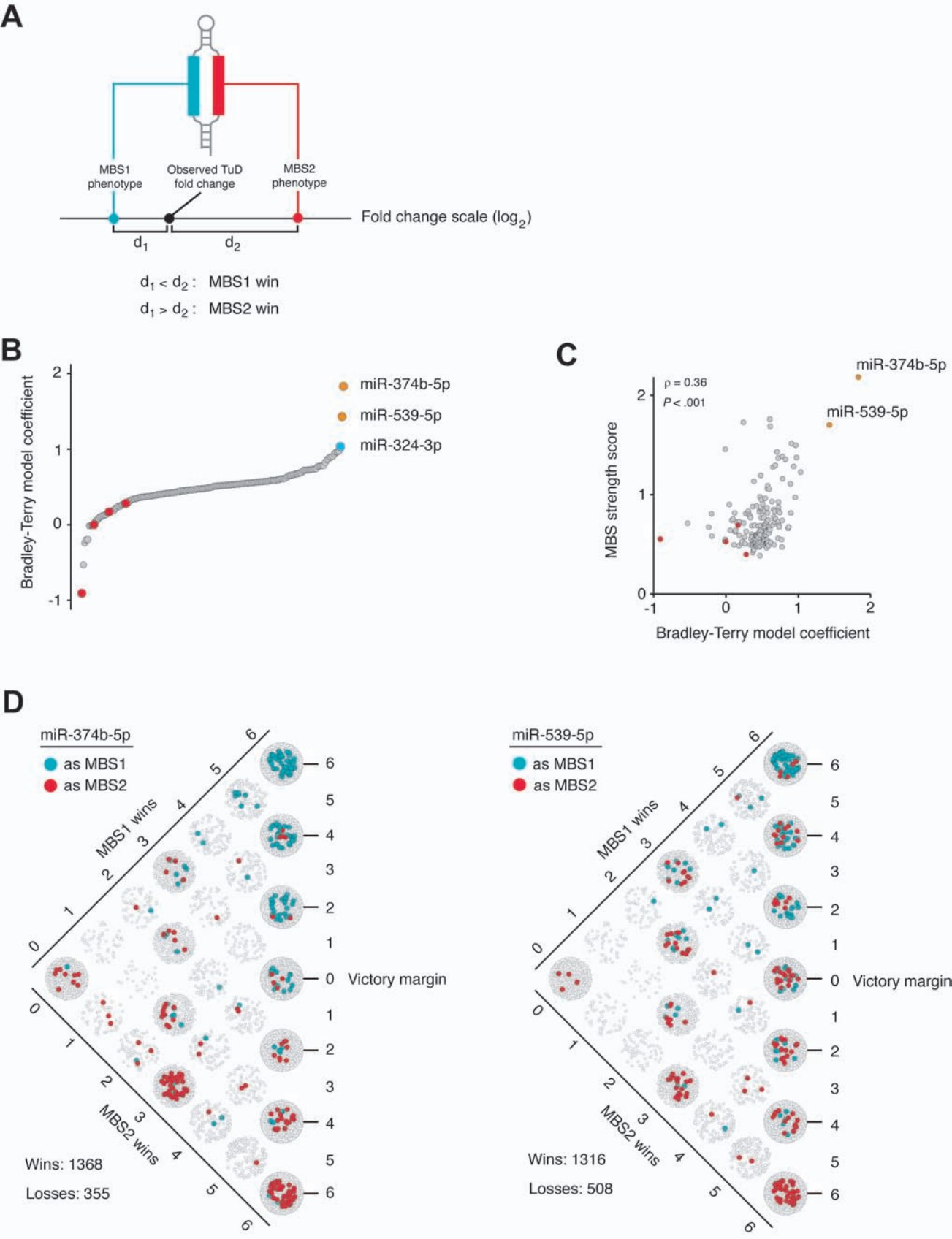
A
MBS1 phenotype
Observed TuD fold change
MBS2 phenotype
Fold change scale (log2)
d1
d2
d1 < d2 : MBS1 win
d1 > d2 : MBS2 win
B
Bradley-Terry model coefficient
miR-374b-5p
miR-539-5p
miR-324-3p
C
ρ = 0.36
P < .001
miR-374b-5p
miR-539-5p
MBS strength score
Bradley-Terry model coefficient
D
miR-374b-5p
as MBS1
as MBS2
MBS1 wins
MBS2 wins
Victory margin
Wins: 1368
Losses: 355
miR-539-5p
as MBS1
as MBS2
MBS1 wins
MBS2 wins
Victory margin
Wins: 1316
Losses: 508

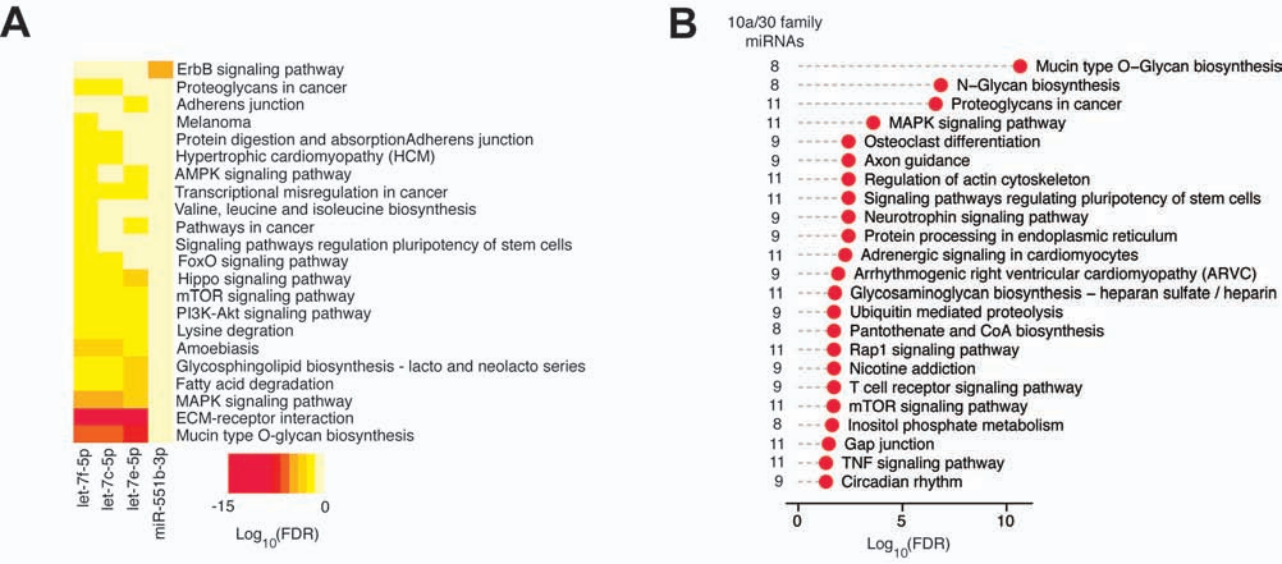
A
ErbB signaling pathway
Proteoglycans in cancer
Adherens junction
Melanoma
Protein digestion and absorptionAdherens junction
Hypertrophic cardiomyopathy (HCM)
AMPK signaling pathway
Transcriptional misregulation in cancer
Valine, leucine and isoleucine biosynthesis
Pathways in cancer
Signaling pathways regulation pluripotency of stem cells
FoxO signaling pathway
Hippo signaling pathway
mTOR signaling pathway
PI3K-Akt signaling pathway
Lysine degration
Amoebiasis
Glycosphingolipid biosynthesis - lacto and neolacto series
Fatty acid degradation
MAPK signaling pathway
ECM-receptor interaction
Mucin type O-glycan biosynthesis
let-7f-5p
let-7c-5p
let-7e-5p
miR-551b-3p
-15
0
Log10(FDR)
B
10a/30 family miRNAs
8 Mucin type O–Glycan biosynthesis
8 N–Glycan biosynthesis
11 Proteoglycans in cancer
11 MAPK signaling pathway
9 Osteoclast differentiation
9 Axon guidance
11 Regulation of actin cytoskeleton
11 Signaling pathways regulating pluripotency of stem cells
9 Neurotrophin signaling pathway
9 Protein processing in endoplasmic reticulum
11 Adrenergic signaling in cardiomyocytes
9 Arrhythmogenic right ventricular cardiomyopathy (ARVC)
11 Glycosaminoglycan biosynthesis – heparan sulfate / heparin
9 Ubiquitin mediated proteolysis
8 Pantothenate and CoA biosynthesis
11 Rap1 signaling pathway
9 Nicotine addiction
9 T cell receptor signaling pathway
11 mTOR signaling pathway
8 Inositol phosphate metabolism
11 Gap junction
11 TNF signaling pathway
9 Circadian rhythm
0
5
10
Log10(FDR)

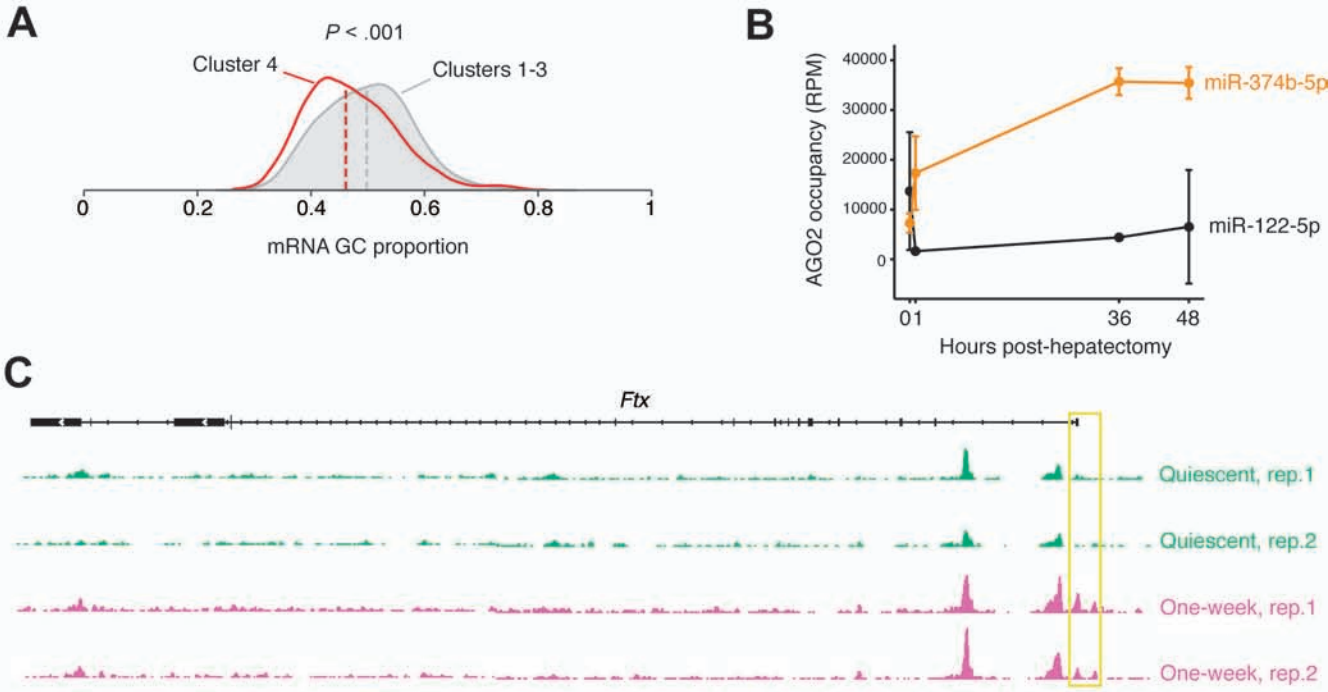
A
P < .001
Cluster 4
Clusters 1-3
0
0.2
0.4
0.6
0.8
1
mRNA GC proportion
B
AGO2 occupancy (RPM)
40000
30000
20000
10000
0
miR-374b-5p
miR-122-5p
01
36
48
Hours post-hepatectomy
C
Ftx
Quiescent, rep.1
Quiescent, rep.2
One-week, rep.1
One-week, rep.2

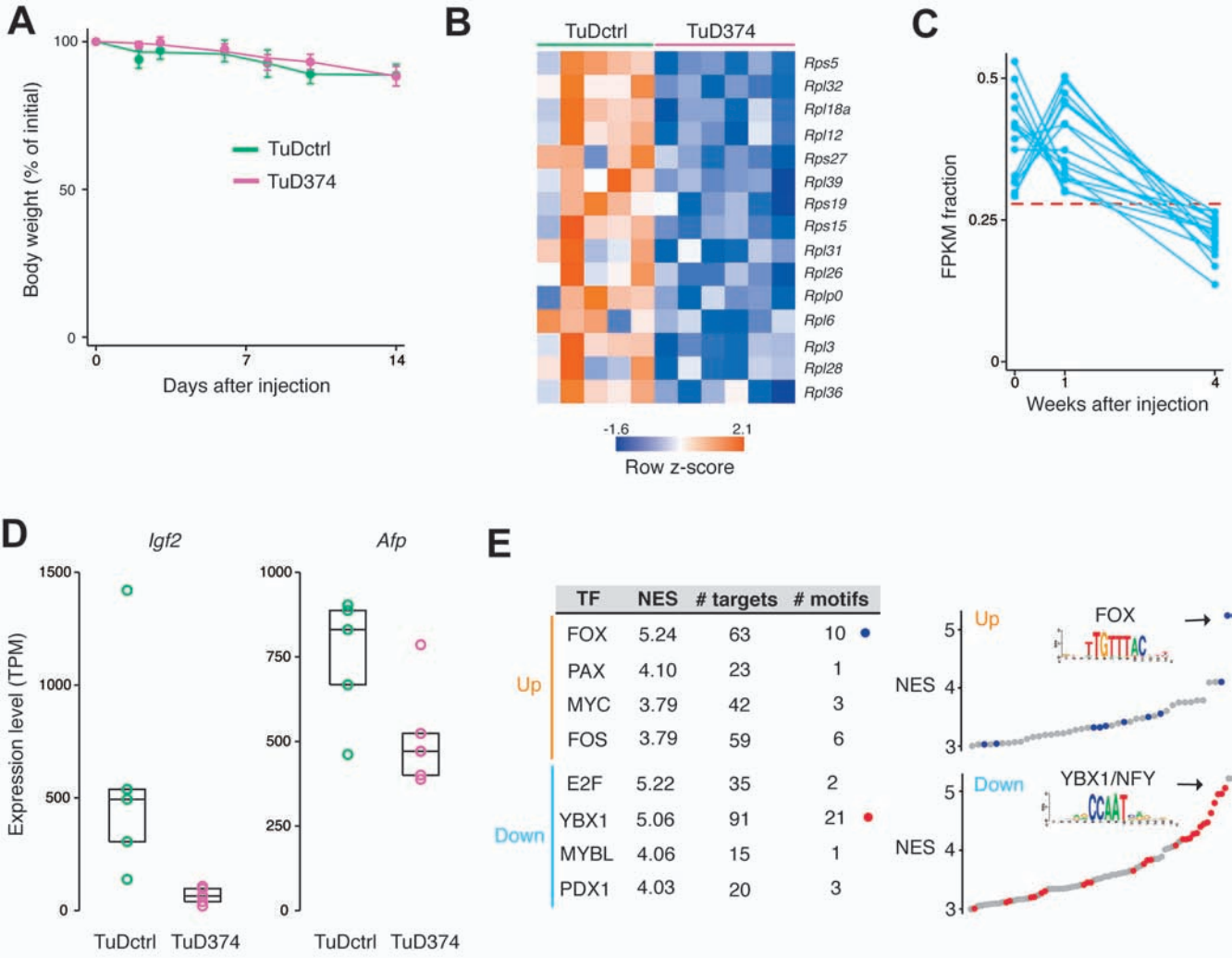
A
Body weight (% of initial)
100
50
0
TuDctrl
TuD374
0
7
14
Days after injection
B
TuDctrl
TuD374
Rps5
Rpl32
Rpl18a
Rpl12
Rps27
Rpl39
Rps19
Rps15
Rpl31
Rpl26
Rplp0
Rpl6
Rpl3
Rpl28
Rpl36
-1.6
2.1
Row z-score
C
FPKM fraction
0.5
0.25
0
0
1
4
Weeks after injection
D
Igf2
Afp
Expression level (TPM)
1500
1000
500
0
1000
750
500
250
0
TuDctrl
TuD374
TuDctrl
TuD374
E
TF
NES
targets
motifs
Up
FOX
5.24
63
10
PAX
4.10
23
1
MYC
3.79
42
3
FOS
3.79
59
6
Down
E2F
5.22
35
2
YBX1
5.06
91
21
MYBL
4.06
15
1
PDX1
4.03
20
3
Up
FOX
NES
5
4
3
Down
YBX1/NFY
NES
5
4
3